

Article

# Coupled Harmonic Admittance Identification Based on Least Square Estimation

Yaqiong Li \*, Zhanfeng Deng, Tongxun Wang, Guoliang Zhao and Shengjun Zhou

State Key Laboratory of Advanced Power Transmission Technology, Global Energy Interconnection Research Institute (GEIRI), Beijing 102209, China; dengzhanfeng@geiri.sgcc.com.cn (Z.D.);

txwang@geiri.sgcc.com.cn (T.W.); zhaoguoliang@geiri.sgcc.com.cn (G.Z.); zhshj@geiri.sgcc.com.cn (S.Z.)

\* Correspondence: liyaqiong@geiri.sgcc.com.cn; Tel.: +86-010-6660-1241

Received: 27 August 2018; Accepted: 26 September 2018; Published: 29 September 2018



**Abstract:** Norton equivalent circuit is a commonly used model in estimating harmonic current emissions of harmonic sources. It however cannot reflect the mutual coupling relationships among voltage and current in different harmonic orders. This paper proposes a new method to identify parameters in a coupled harmonic admittance model. The proposed method is conducted using voltage and current measurements and is based on least square estimation technique. The effectiveness of the method is verified through time-domain simulations for a grid-connected converter and also through field data obtained from a  $\pm 800$  kV converter station. The experimental results showed that the proposed method presents higher accuracy in terms of harmonic current emission estimation compared with three Norton-base methods.

**Keywords:** harmonic admittance; Norton model; harmonic state estimation; recursive parameter identification

## 1. Introduction

In recent years, with the increasing penetration of distributed energy and nonlinear loads, harmonics have attracted much attention of both grid operators and power users. Modeling of harmonic sources is essential in estimating the harmonic current contribution as a function of the background harmonic voltage. Authors in Reference [1] summarized the progress in harmonic analysis in both time and frequency domains. Among the state-of-the-art harmonic modeling methods, Norton model is a commonly-used equivalent circuit of harmonic sources [2–7]. Authors in References [8,9] built Norton's equivalent circuit for iron and steel plants and estimated their harmonic current contributions to the background grid. In Reference [10], the authors considered the open-loop inverter of a double-stage PV system as a Norton equivalent. Paper [11] estimated the shares and locations of harmonic sources in radial distribution systems using the Norton model as representation of the customer side. A discrete time-domain closed-loop Norton's equivalent circuit is developed in Reference [12] for a micro-grid. Paper [13] analyzed Inverse Nyquist Stability Criterion for a grid-tied inverter system based on a Norton equivalent circuit of the inverter.

Parameters in Norton models can be derived in analytical forms based on circuit topology and control schemes associated with harmonic sources. In Reference [14], the authors considered control-related parameters in building Norton model for a grid-tied inverter and justified the method through a case study on a 1.4 MW PV plant. Impedance-based Norton modelling is studied in Reference [15] for a VSC-HVDC (Voltage Source Converter High Voltage Direct Current) system and the impact of the different parameters on the system dynamics and stability is also analyzed.

The analytical derivation of Norton parameters cannot match the operational conditions due to aging of the system modules as well as time-varying characteristic of the system parameters.

For example, paper [16] addressed that the accuracy of Norton parameter evaluation for a PV plant are affected by aging of the PV modules. To address the time-varying feature of harmonic characteristics, paper [17] used iterative Norton modelling to make customer harmonic emission levels assessment. Independent component analysis is used to describe the stochastic feature of Norton parameters in Reference [18].

In case of absence of control parameters involved in analytical derivation of Norton, small-signal impedance modeling is an alternative way of modelling parameter estimation. In Reference [19], Authors excited the system with short sequences of current signals and identified its impedance by constructing the relationship between corresponding voltage and current characteristics. A study in Reference [20] is conducted using this method to analyze the terminal characteristics of a MMC (Modular Multilevel Converter) system. In Reference [21], a defined current pulse is injected into the medium-voltage network and the network impedance is then evaluated by analyzing the network voltage responses. Authors in Reference [22] developed a harmonic matrix of the grid-connected converter using a Harmonic State Space (HSS) small signal model, with considerations of its time-varying feature. In Reference [23], different control schemes are considered in the HSS-based small-signal impedance modeling for a MMC system.

However, since small-current excitation into the system is required in small-signal impedance modeling, it is difficult to be applied widely due to its practical complexity and costs. Furthermore, as the power quality monitoring system is implemented in many countries [24], the field measurements of voltage and current are quite available. Therefore, identification of Norton parameters using measurements is a practical method. In References [17,25–27], Norton-based harmonic impedance is identified from measurement data using linear estimation method.

Norton model itself in essence is not able to describe the mutual coupling relationships among voltage and current in different harmonic orders. However, this coupling relationship does exist and presents significant impact on the grid [28]. In Reference [29], a cross-frequency admittance model is obtained but the model is found only suitable for specific operational conditions [26].

To address the mutual coupling between harmonics in different orders, authors in References [28,30] proposed a frequency-domain coupled linear admittance matrix and presented its theoretical foundation and analytical derivations. The elements in the admittance matrix are independent of harmonic voltages in the ac side. Based on this model, authors in Reference [31] established the frequency-domain harmonic analytical model for EV charger. Also, frequency-domain analytical model is constructed for home appliances [32] and compact fluorescent lamps in Reference [33].

As aforementioned, the control-related parameters involved in derivation equations are not only time-varying but also hardly obtained. Therefore, constructing the model using measurements is an alternative method. Authors in Reference [26] conducted matrix manipulation for the model and found the manipulation is ill-conditioned. Aiming to solve the ill-conditioning problem, two simplified models are thus built, with one omits the conjugate part of the model and the other simplified into a Norton model. Authors in Reference [27] simplified the model by assuming that there is no distortion in the background voltage. These simplifications decreased the accuracy of the model to some extent. To address this issue, this paper proposed an identification method of the coupled harmonic admittance based on least square estimation using measurement data.

This paper is organized as follows. The proposed harmonic admittance identification technique is described in Section 2. In Section 3, two case studies are presented to evaluate the effectiveness of the proposed method. Discussion of the advantage and disadvantage of the method is described in Section 4. Finally, the conclusion is presented in Section 5.

## 2. Coupled Harmonic Admittance Identification

The coupled harmonic admittance model aims to estimate the harmonic current contribution as a function of the background harmonic voltages. The model builds relationships among current and voltage in all harmonic orders [28], which can be described in the following equation.

$$\mathbf{I} = \mathbf{Y}^+ \mathbf{U} + \mathbf{Y}^- \mathbf{U}^* + \mathbf{I}^0 \quad (1)$$

The compact form in Equation (1) can also be rewritten as follows.

$$\begin{bmatrix} I_1 \\ I_2 \\ I_3 \\ \dots \\ I_H \end{bmatrix} = \begin{bmatrix} Y_{1,1}^+ & Y_{1,2}^+ & Y_{1,3}^+ & \dots & Y_{1,H}^+ \\ Y_{2,1}^+ & Y_{2,2}^+ & Y_{2,3}^+ & \dots & Y_{2,H}^+ \\ Y_{3,1}^+ & Y_{3,2}^+ & Y_{3,3}^+ & \dots & Y_{3,H}^+ \\ \dots & \dots & \dots & \dots & \dots \\ Y_{H,1}^+ & Y_{H,2}^+ & Y_{H,3}^+ & \dots & Y_{H,H}^+ \end{bmatrix} \begin{bmatrix} U_1 \\ U_2 \\ U_3 \\ \dots \\ U_H \end{bmatrix} + \begin{bmatrix} Y_{1,1}^- & Y_{1,2}^- & Y_{1,3}^- & \dots & Y_{1,H}^- \\ Y_{2,1}^- & Y_{2,2}^- & Y_{2,3}^- & \dots & Y_{2,H}^- \\ Y_{3,1}^- & Y_{3,2}^- & Y_{3,3}^- & \dots & Y_{3,H}^- \\ \dots & \dots & \dots & \dots & \dots \\ Y_{H,1}^- & Y_{H,2}^- & Y_{H,3}^- & \dots & Y_{H,H}^- \end{bmatrix} \begin{bmatrix} U_1^* \\ U_2^* \\ U_3^* \\ \dots \\ U_H^* \end{bmatrix} + \begin{bmatrix} I_1^0 \\ I_2^0 \\ I_3^0 \\ \dots \\ I_H^0 \end{bmatrix} \quad (2)$$

where  $\mathbf{U}$  is the vector of fundamental and harmonic voltages,  $\mathbf{U}^*$  is the conjugate value of  $\mathbf{U}$  and  $U_h$  represents the harmonic voltage component in the harmonic order of  $h$ . Similarly,  $I$  is the vector of harmonic currents of different orders and  $I_h$  represents the  $h$ -th harmonic current.  $H$  is the maximum harmonic order of interest. In the strict mathematical form, the highest order of current and voltage can be different. However, since the paper aims to estimate the admittance matrix based on measurement data, so the highest harmonic orders for voltage and current are considered the same.

The admittance matrix, that is,  $Y^+$ ,  $Y^-$ , together with the current source  $I^0$ , are the linear parameters between current and voltage in all harmonic orders. The combination of  $Y_{n,h}^+$  and  $Y_{n,h}^-$  represent the coupled admittance between  $h$ -th harmonic voltage and  $n$ -th harmonic current.

It is clear that the model couples all harmonic voltages and current components, that is, each harmonic voltage has contributions to harmonic currents at all frequencies. Additionally, the coupled matrix indicates that the harmonic current is a function of both the voltage itself and its conjugate.

In order to estimate the unknown admittance  $Y^+$ ,  $Y^-$  and current source  $I^0$ , [26] derived a method based on matrix manipulation. However, it was found and also evidenced in our experiment that, this method is vulnerable to numerical difficulties since the manipulated matrix is ill-conditioned for most of the data. To conquer this problem, a method based on Least Square Estimation (LSE) is proposed in this paper.

Also, it should be noticed that Norton model is actually a simplification of the coupled admittance model. By removing the conjugate counterpart of the voltage, as well as the admittance between different frequencies, the Norton model can be described as below.

$$\begin{bmatrix} I_1 \\ I_2 \\ I_3 \\ \dots \\ I_H \end{bmatrix} = \begin{bmatrix} Y_{1,1}^+ & 0 & 0 & \dots & 0 \\ 0 & Y_{2,2}^+ & 0 & \dots & 0 \\ 0 & 0 & Y_{3,3}^+ & \dots & 0 \\ \dots & \dots & \dots & \dots & \dots \\ 0 & 0 & 0 & \dots & Y_{H,H}^+ \end{bmatrix} \begin{bmatrix} U_1 \\ U_2 \\ U_3 \\ \dots \\ U_H \end{bmatrix} + \begin{bmatrix} I_1^0 \\ I_2^0 \\ I_3^0 \\ \dots \\ I_H^0 \end{bmatrix} \quad (3)$$

For comparison, three Norton-based identification methods are conducted in the experiments. Details of the methods are included in Section 3.

Based on Equation (2), the  $h$ -th harmonic current  $I_h$  and the  $h$ -th harmonic voltage  $U_h$  are first divided into their real and imaginary parts, as indicated in Equation (4). Note that  $i_h$  and  $\tilde{i}_h$  are

the real and imaginary part of  $I_h$ , respectively. The same rule applies to  $U_h, Y_{n,h}^+, Y_{n,h}^-$  and  $I_h^0$ . Here  $n, h = 1, \dots, H$ .

$$\begin{aligned}
 I_h &= i_h + \tilde{i}_h \cdot j & \mathbf{I} &= \mathbf{I} + j \cdot \tilde{\mathbf{I}} \\
 U_h &= u_h + \tilde{u}_h \cdot j & \mathbf{U} &= \mathbf{U} + j \cdot \tilde{\mathbf{U}} \\
 Y_{n,h}^+ &= Y_{n,h}^+ + \tilde{Y}_{n,h}^+ \cdot j & \Leftrightarrow \mathbf{Y}^+ &= \mathbf{Y}^+ + j \cdot \tilde{\mathbf{Y}}^+ \\
 Y_{n,h}^- &= Y_{n,h}^- + \tilde{Y}_{n,h}^- \cdot j & \mathbf{Y}^- &= \mathbf{Y}^- + j \cdot \tilde{\mathbf{Y}}^- \\
 I_h^0 &= i_h^0 + \tilde{i}_h^0 \cdot j & \mathbf{I}^0 &= \mathbf{I} + j \cdot \tilde{\mathbf{I}}^0
 \end{aligned}
 \tag{4}$$

By separating the real and imaginary part of each element, Equation (2) can be represented in the following forms.

$$i_h = \sum_{n=1}^H \left[ \underbrace{(y_{n,h}^+ + y_{n,h}^-)}_{a_{n,h}} u_n + \underbrace{(\tilde{y}_{n,h}^- - \tilde{y}_{n,h}^+)}_{b_{n,h}} \tilde{u}_h \right] + i_h^0
 \tag{5}$$

$$\tilde{i}_h = \sum_{n=1}^H \left[ \underbrace{(\tilde{y}_{n,h}^+ + \tilde{y}_{n,h}^-)}_{c_{n,h}} u_n + \underbrace{(y_{n,h}^+ - y_{n,h}^-)}_{d_{n,h}} \tilde{u}_h \right] + \tilde{i}_h^0
 \tag{6}$$

As indicated in the above equation, let  $a_{n,h} = y_{n,h}^+ + y_{n,h}^-$ . The same rule also applies to  $b_{n,h}, c_{n,h}$  and  $d_{n,h}$ .

After obtaining  $M$  measurements of voltage and current harmonic components, Equation (7) can be obtained, according to Equation (5).

$$\underbrace{\begin{pmatrix} i_h^{(1)} \\ i_h^{(2)} \\ \vdots \\ i_h^{(M)} \end{pmatrix}}_A = \underbrace{\begin{pmatrix} u_1^{(1)} & u_2^{(1)} & \dots & u_H^{(1)} & \tilde{u}_1^{(1)} & \tilde{u}_2^{(1)} & \dots & \tilde{u}_H^{(1)} & 1 \\ u_1^{(2)} & u_2^{(2)} & \dots & u_H^{(2)} & u_1^{(2)} & u_2^{(2)} & \dots & u_H^{(2)} & 1 \\ \vdots & \vdots & \ddots & \vdots & \vdots & \vdots & \ddots & \vdots & 1 \\ u_1^{(M)} & u_2^{(M)} & \dots & u_H^{(M)} & u_1^{(M)} & \tilde{u}_2^{(M)} & \dots & u_H^{(M)} & 1 \end{pmatrix}}_X \underbrace{\begin{pmatrix} a_{1,h} \\ a_{2,h} \\ \vdots \\ a_{H,h} \\ b_{1,h} \\ b_{2,h} \\ \vdots \\ b_{H,h} \\ i_h^0 \end{pmatrix}}_B
 \tag{7}$$

Note that Equation (7) is in the form of  $A = XB$ . To solve this linear equation, LSE can be used to obtain the estimations of unknown parameters in Equation (5).

$$B = (X^T X)^{-1} X^T A
 \tag{8}$$

LSE is able to produce estimation values of  $a_{n,h}, b_{n,h}, c_{n,h}, d_{n,h}$  and current sources  $i_h^0$  and  $\tilde{i}_h^0$ . Using estimation values of  $a_{n,h}, b_{n,h}, c_{n,h}$  and  $d_{n,h}$ , Equation (9) can be calculated to obtain the real and imaginary parts of the two harmonic admittance matrix.

$$\begin{aligned}
 y_{n,h}^+ &= (a_{n,h} + d_{n,h})/2 \\
 \tilde{y}_{n,h}^+ &= (b_{n,h} - c_{n,h})/2 \\
 y_{n,h}^- &= (a_{n,h} - d_{n,h})/2 \\
 \tilde{y}_{n,h}^- &= (b_{n,h} + c_{n,h})/2
 \end{aligned}
 \tag{9}$$

Similarly, LSE can also be used to derive the admittance and current source in Equation (6).

Therefore,  $Y^+$ ,  $Y^-$  and  $I^0$  can be derive. After identification of harmonic admittance matrix and current sources, estimation of harmonic current can then be obtained given the grid voltage with or without distortion.

As indicated in Reference [28], the elements of coupled admittance matrix are sensitive to the changes of parameters such as firing angle of a converter. To describe the time-varying characteristic of related parameters, a recursive method is constructed to obtain the changing values of elements in the coupled matrix.

The time series of measurement are divided into  $M$  groups in chronological order. For each group of measurements, the two admittance matrix together with current source are constructed using the identification method mentioned above. Here, let  $\dot{Y}_M$  be the unified notation for two admittance matrix and one current source estimated using measurements of the  $M$ -th group. Then, the final estimations for each group can be built in the following recursive form.

$$\begin{aligned}\dot{Y}_M &= (1 - \varepsilon)Y_M + \varepsilon Y_{M-1} \\ &= (1 - \varepsilon)Y_M + (1 - \varepsilon)\varepsilon^j Y_{M-j} + \dots + \varepsilon^{M-1} Y_1 \quad j = 1, 2, \dots, M - 1\end{aligned}\quad (10)$$

where  $\varepsilon$  is a forgetting factor ranging from 0 to 1. Smaller value of this factor is more suitable for situations with parameters of less variations. Using Equation (10), the effect of the past measurements is fading gradually and the most recent measurement contributes most to the estimation, thus achieving accuracy of the harmonic current estimation.

### 3. Case Studies

#### 3.1. Norton-Based Methods for Comparison

Norton model, as indicated in Equation (3), is used to compare with the proposed method. The identification of parameters in Norton is carried out using three methods. One of them is traditional two-point method [34], which calculates the admittance as the ratio of derivation of current to the deviation of voltage between two measurements. Another is based on matrix manipulation as described in Reference [26]. In the third method, the real and imaginary parts of the Norton model are separated first. LSE is carried out for the real part to estimate the admittance, then the current source is obtained through combination with the equation for imaginary part [17]. The three methods are named as Norton-two points, manipulation and LSE respectively and are conducted in the following experiments.

#### 3.2. Experimental Results by Matlab/Simulink Simulation

To verify the accuracy of the proposed coupled harmonic admittance identification method, a time-domain simulation for a single-phase bridge converter is conducted using Matlab/Simulink platform. Figure 1 shows the schematic circuit and Figure 2 shows the circuit topology in simulations.

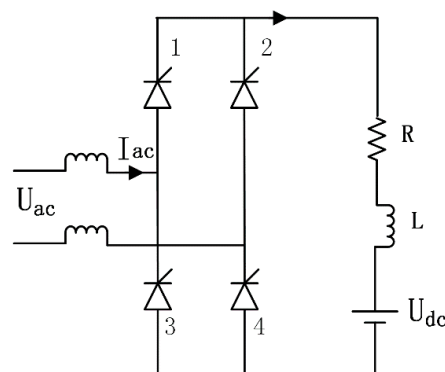


Figure 1. Schematic circuit of a single-phase bridge converter.

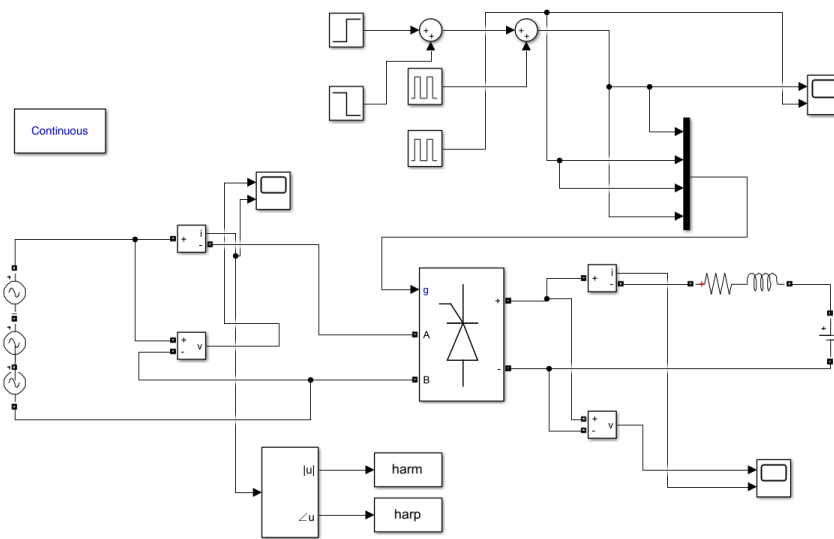


Figure 2. Circuit topology in Matlab/Simulink simulation.

According to the theoretical analysis [28], the elements of the coupled admittance matrix are related with fundamental voltage phase and parameters of the converter such as firing angle but independent of harmonic voltages at ac side. Therefore, in the simulations, the parameters involved in the matrix are made fixed, as shown in Table 1, while the harmonic voltage components vary in order to obtain enough samples for estimation.

Table 1. Fixed experimental parameters involved in the simulations.

Parameter	Value	Parameter	Value
Fundamental phase	30	Edc(V)	25
R(Ohm)	1	Firing angle (°)	60
L(H)	0.001	Firing pulse width	%10 cycle

As indicated in Table 2, 60 simulations are carried out. The harmonic voltage and current components are extracted from the steady state of those simulations using Fast Fourier Transform (FFT) and treated as measurements. The first 50 simulations are used for training and the last 10 for testing. Both 3rd and 5th harmonic components are included in the voltage at ac side and their magnitudes and phases are kept changing.

Table 2. Changing harmonic voltage components in 60 simulations.

No.	Funda-Mental (V)	3rd Voltage (%)	3rd Phase (°)	5th Voltage (%)	5rd Phase (°)
1–10	130:10:220	40	20	25	50
11–20	220	12:2:30	20	25	50
21–30	220	40	12:2:30	25	50
31–40	220	40	20	11:1:20	50
41–50	220	40	20	25	4:4:40
51–60	135:10:225	13:2:31	11:2:29	10.5:1:19.5	3:4:39

Figure 3 shows the comparisons between harmonic voltages and currents in the ac side for one simulation. The resistance R is set as one and the reactance is set low, making the values of harmonic voltages and currents quite close. It can be found that although there are no voltage components in orders higher than three, 5th and higher harmonic currents still exist. This clearly evidenced the mutual coupling between harmonic voltage and current in different orders.

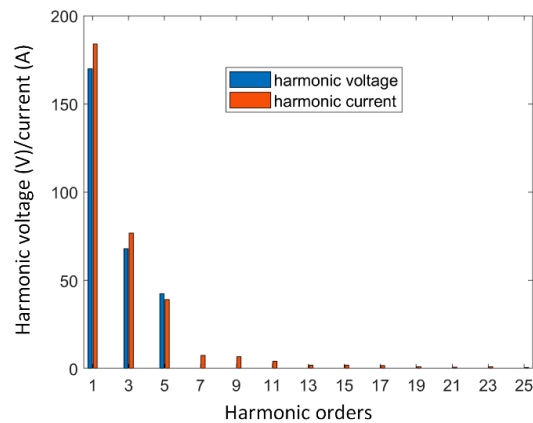


**Figure 3.** Harmonic voltage and current components in the ac side of the converter.

The admittance and current source are estimated using the voltage and current measurements from the first 50 simulations. Figure 4 shows the values of elements in the two admittance matrix, that is,  $Y^+$  and  $Y^-$ . It can be seen that as to  $Y^+$ , 3rd harmonic voltage contributes most to the 3rd harmonic current, while the same phenomenon happens for 5th harmonics. However, as to  $Y^-$ , fundamental voltage contributes most the 3rd harmonic current. Further, the contributions of  $Y^+U$ ,  $Y^-U^*$  and  $I^0$  are presented in Figure 5. Even though the part of  $Y^-U^*$  is commonly omitted in the state-of-the-art methods, Figure 5b clearly shows that the contribution of  $Y^-U^*$  cannot be ignored.

Using the admittance and current source estimated from the first 50 simulations, the harmonic currents are predicted for the final 10 simulations and compared with the measurements. Figure 6 illustrates the comparisons of predicted 3rd and 5th harmonic currents by proposed method and also by three Norton-based ones. The method of Norton-two points showed biggest deviations from the actual measurements. Among the predictions made by the four methods, the one by the proposed method are well consistent with the measurements.

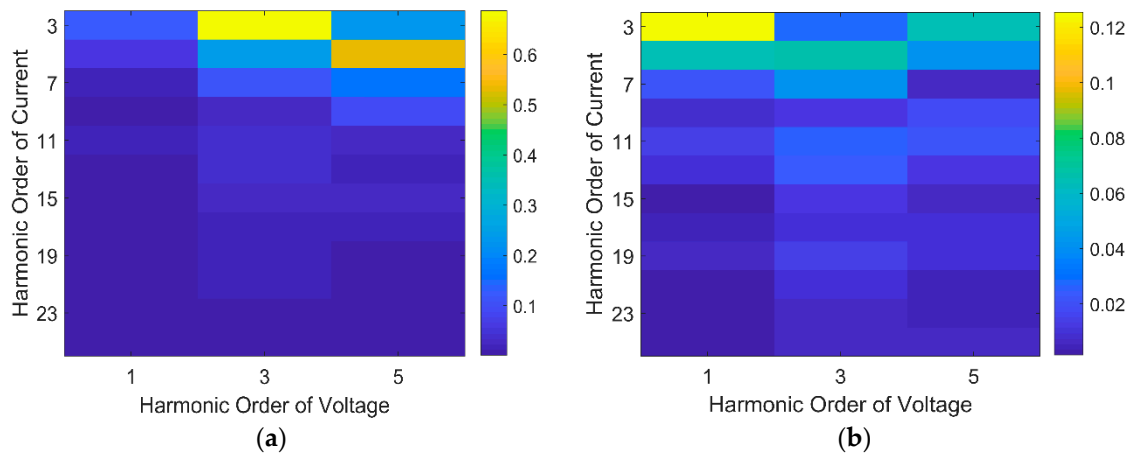


**Figure 4.** Magnitude of estimated admittance model  $Y^+$  (a) and  $Y^-$  (b), with unit Ohms.

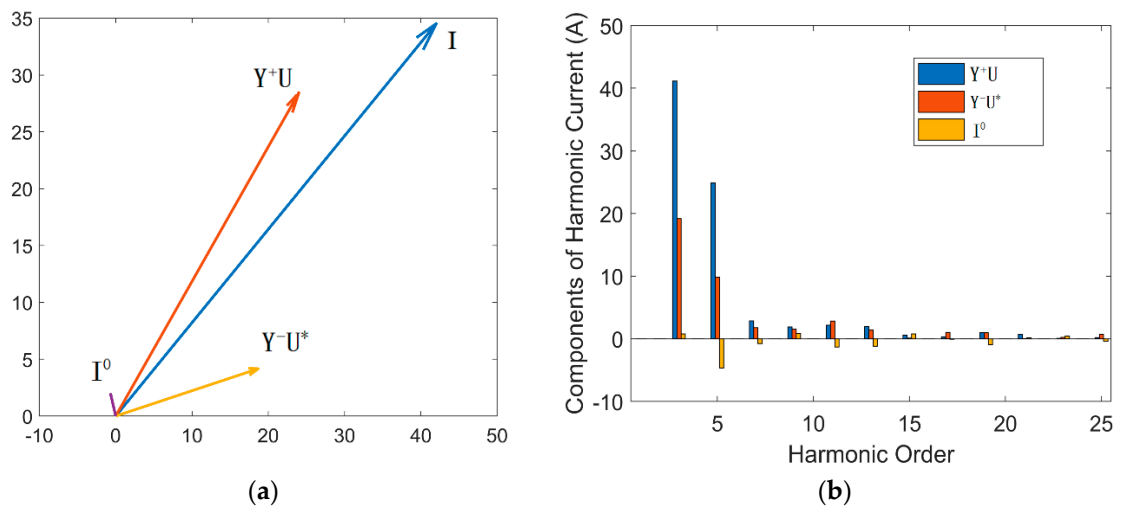


**Figure 5.** Three components of estimated harmonic current, that is,  $Y^+$ ,  $Y^-$  and  $I^0$  respectively. Three components of one 3rd harmonic current vector estimation (a) and three components for estimation harmonic current in orders from 3 to 25 (b).

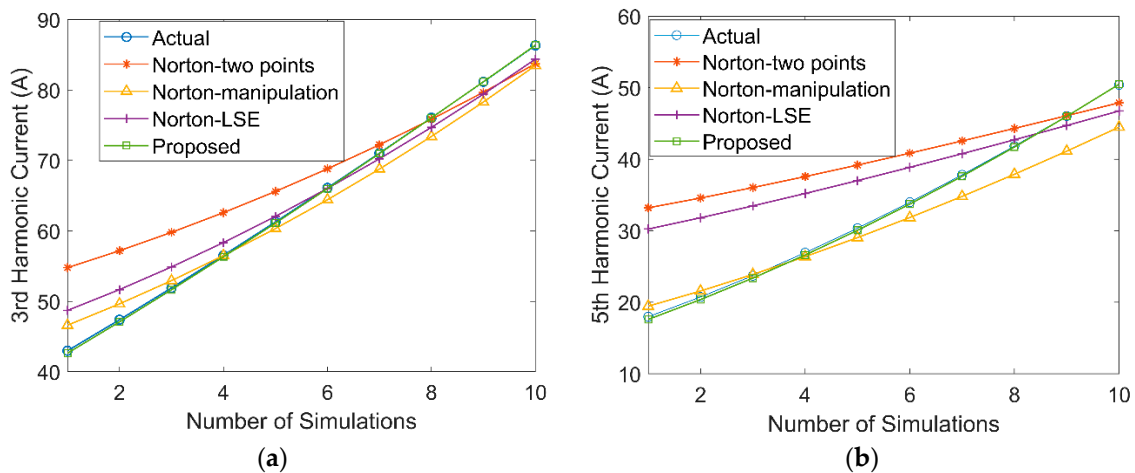


**Figure 6.** Comparisons of 3rd (a) and 5th (b) harmonic current estimation by proposed method and Norton-based methods.

To quantify the performance of proposed method and Norton-based methods, RMSE (Root Mean Square Error) and MAE (Mean Absolute Error) are calculated. RMSE and MAE measure the accuracy of the predictions. The lower their values, the more accurate the predictions. Let  $m_i$  be the  $i$ -th measurement and  $p_i$  be the  $i$ -th prediction,  $i = 1, 2, \dots, N$ . RMSE and MAE can be calculated as follows.

$$RMSE = \sqrt{\frac{1}{N} \sum_{i=1}^N (m_i - p_i)^2} \tag{11}$$

$$MAE = \frac{1}{N} \sum_{i=1}^N |m_i - p_i| \tag{12}$$

Tables 3 and 4 present the prediction errors of four methods for 3rd and 5th harmonic orders with regard to RMSE and MAE. It can be seen that the two-point method gave the worst performance, the method of Norton LSE and manipulation gave better performance than the two-point method. The proposed method shows highest prediction accuracy compared with three Norton based methods.

**Table 3.** Comparisons between the proposed method and Norton-based methods for 3rd harmonic current w.r.t. RMSE and MAE.

	Norton-Two Points	Norton-Manipulation	Norton-LSE	Proposed
RMSE	6.08	2.26	2.70	0.19
MAE	4.80	2.02	2.15	0.15

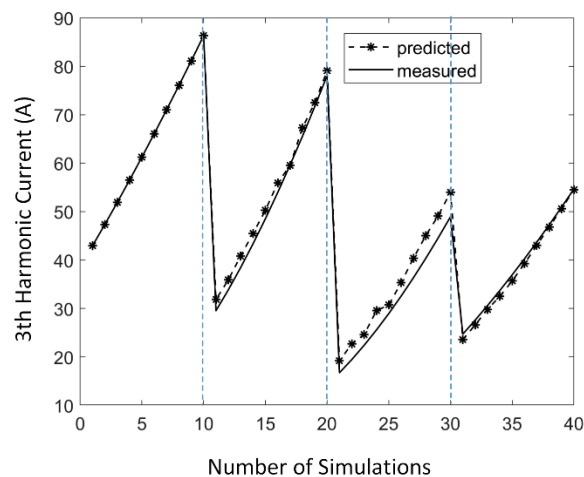
**Table 4.** Comparisons between the proposed method and Norton-based methods for 5th harmonic current w.r.t. RMSE and MAE.

	Norton-Two Points	Norton-Manipulation	Norton-LSE	Proposed
RMSE	9.21	3.05	7.27	0.26
MAE	7.74	2.42	6.17	0.23

In order to verify the proposed recursive method, an additional simulation is designed, which changes all parameters related or unrelated with the elements of admittance matrix. Forty simulations are conducted. The experimental parameters in the aforementioned testing are used in the first 10 simulations. Table 5 presents the parameter settings for the following 30 simulations. The values of firing angle and resistance change three times, as indicated by dashed lines in Figure 7.

**Table 5.** Changing experimental parameters and harmonic voltage components in simulations.

Simulation No.	11–20	21–30	31–40
Firing Angle (°)	60	30	20
R(Ohm)	1	1.2	2
Fundamental RMS (V)	135:10:225	135:10:225	135:10:225
3rd Voltage (%)	13:02:31	13:02:31	13:02:31
3rd Voltage Phase (°)	11:02:29	11:02:29	11:02:29
5th Voltage (%)	10.5:1:19.5	10.5:1:19.5	10.5:1:19.5
5th Voltage Phase (°)	3:04:39	3:04:39	3:04:39

**Figure 7.** 3th harmonic current estimation by proposed recursive method.

In generating harmonic predictions, the measurements of 40 simulations are divided into five groups, with each group containing eight measurements. The forgetting factor is set as 0.2. Figure 7 shows the variations of predicted harmonic currents using recursive identification method. Dashed lines represent the time stamps with parameters changing. The 3rd harmonic current estimations by the recursive method show deviations from measurement to some degree, especially at the time of admittance-related parameters changing. However, the deviations are narrowed gradually along with time. Also, after applying other values of forgetting factor, similar results with Figure 7 are

obtained. Considering the overall pattern between results of recursive identification and measurements, the current predictions made by recursive method are quite consistent with the measurements.

### 3.3. Experimental Results for Field Data

To verify the accuracy of the proposed method, the measurements obtained from a converter station is used [35]. The converter station connected with a  $\pm 800$  kV UHVDC (Ultra High Voltage Direct Current) power transmission line and is constructed by four 12-pulse valves.

Measurements are available for three locations in the converter station—converter transformer, filter branch and AC network sides respectively. A number of waveform recordings with duration of six to ten seconds and with sampling rate of 10 kHz are used to verify the effectiveness of the proposed method. The measurements are made using on-site monitoring terminals and be obtained through a power quality monitoring system [24].

Figure 8 shows the comparisons between the harmonic current of two monitoring sites, located in converter transformer and AC network side separately. For both monitoring points, 5th, 11th, 13th, 23th and 25th harmonic current contents, together with high-frequency harmonics such as 35th, 38th and 39th, are significant compared with harmonic current in other orders. The 11th and 13th harmonic current on AC side is much lower than that on transformer side, due to the effect of filter branches. The 5th and 39th harmonic current emissions on AC side are even larger than that on transformer side, probably due to the accumulation effect made by several transformer branches.

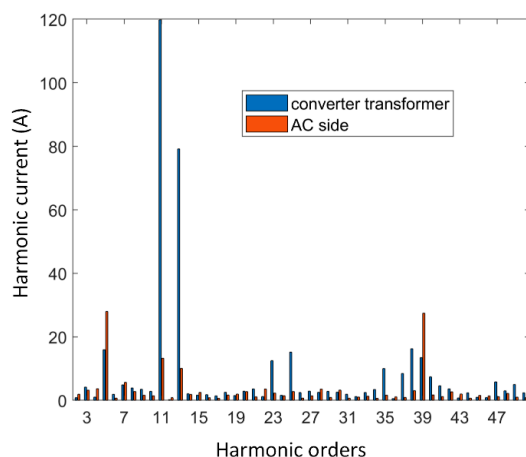


**Figure 8.** Comparisons of harmonic current components between monitoring points located in converter transformer and AC side.

The voltage and current waveform data of monitoring points located at converter transformer is extracted and its harmonic components are identified using FFT. The DC, fundamental and 2–50th harmonic components are all extracted. In the following figures, the results for Phase A is illustrated as an example.

To estimate the two coupled harmonic admittance matrix and one current source in Equation (2), at least 100 measurements are required, given that the maximum harmonic order in consideration is set as 50. Each measurement should contain 1~50th harmonic voltage and current components. Here, the window width for FFT is chosen as one cycle. Therefore, the admittance is first identified using the harmonic components from the 100 cycles and then be used to estimate the harmonic current for the neighboring 50 cycles.

The admittance matrix, that is,  $Y^+$  and  $Y^-$ , are estimated and shown in Figure 9. It shows that the admittance of 39th is relatively high, indicating that it has potential of harmonic resonance in this order. In addition, there is no obvious diagonal stripe in the figures, therefore, the background voltage in the same order does not contribute most to the harmonic current.

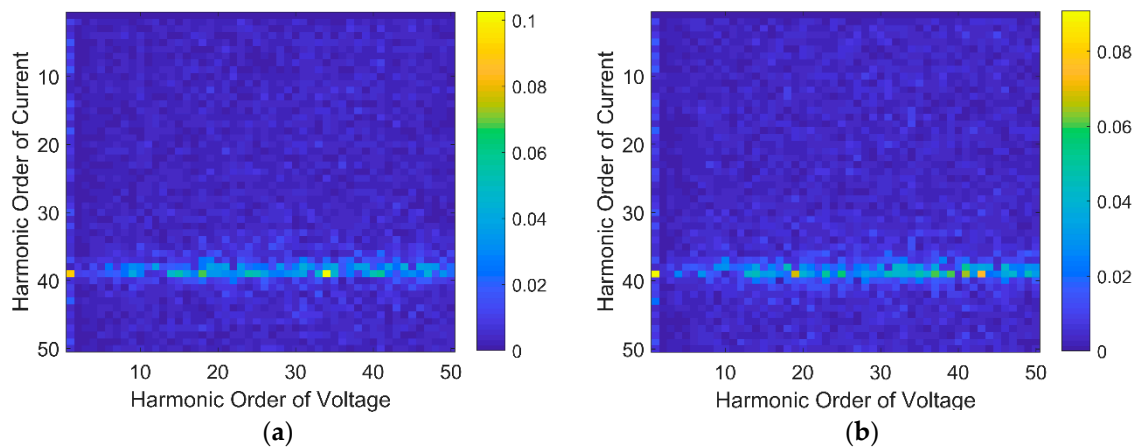


Figure 9. Magnitude of estimated admittance model  $Y^+$  (a) and  $Y^-$  (b), with unit Ohms.

The admittance and harmonic source calculated using the proposed method are used to estimate the harmonic currents. Estimations from three Norton-based methods are used for comparison. To quantify their performance, THDi (Total Harmonic Distortion for Current) is calculated, using the following equation [36].

$$THD_i = \frac{\sqrt{\sum_{h=2}^H I_h^2}}{I_f} \times 100\% \tag{13}$$

where  $I_f$  represents fundamental current RMS (Root Mean Square) value and  $I_h$  is RMS of  $h$ -th harmonic current, the highest harmonic order in consideration is 50.

Figure 10 shows comparisons between different methods. It can be seen that THDi produced by method of Norton-two points and manipulation is approximately 1% higher than the actual ones. Norton-LSE method and the proposed method both gave better performance. In detail, Norton-LSE method gave relatively invariant estimations for the whole time period, while the THDi produced by the proposed method shows a similar pattern to the actual ones.

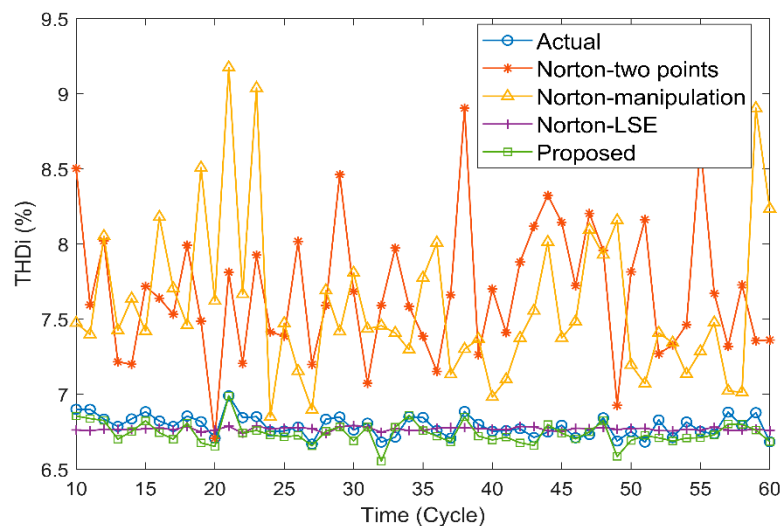
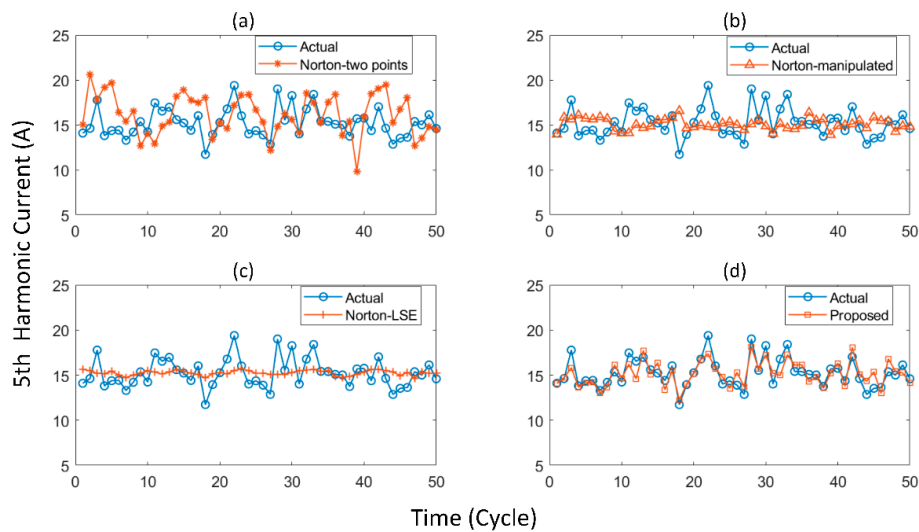
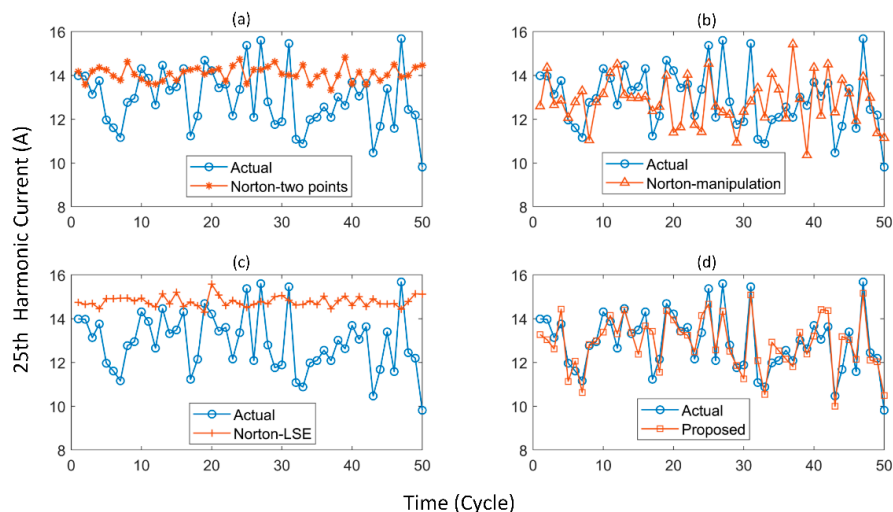


Figure 10. Comparisons of estimation of THDi by proposed method and Norton-based methods.

Figures 11 and 12 present the comparisons of estimated 5th and 25th harmonic current by the proposed method and three Norton-based methods. The former one shows a highly consistent pattern with the measured currents, while the other methods present a worse performance, which either fluctuate around the average value or shows a different variation pattern.



**Figure 11.** Comparisons of 5th harmonic current between actual measurement and estimations by Norton-two point method (a), Norton-manipulated method (b), Norton-LSE method (c) and the proposed method (d).



**Figure 12.** Comparisons of 25th harmonic current between actual measurement and estimations by Norton-two point method (a), Norton-manipulated method (b), Norton-LSE method (c) and the proposed method (d).

To quantify the performance of the four methods, RMSE and MAE are calculated for a number of waveform data measured on transformer side. Besides, Pearson's Correlation Coefficient is also calculated, which measures the correlation of two variables. The closer the value to one, the stronger correlation the two variables have, indicating higher accuracy.

Tables 6–8 present the estimation errors of the two methods for 3rd–25th odd harmonics with regard to RMSE, MAE and Pearson's Correlation Coefficient. It can be derived that for all three metrics, the proposed method shows highest estimation accuracy. Especially for Pearson's Correlation Coefficient, the proposed method presented values closer to 1, while the other three methods gave values near zero. This result clearly shows that the harmonic current estimations of the proposed method are quite consistent with the actual ones.

Additionally, to compare the computational efficiency of the four methods, the computation time consumed by the four methods for the two case studies are compared, as in Table 9. The computation time of the proposed method is approximately three times of that of the other three methods.

**Table 6.** Comparisons between the proposed method and Norton-based methods w.r.t. RMSE.

	3rd	5th	7th	9th	11th	13th	15th	17th	19th	21th	23th	25th
<b>Norton-Two points</b>	4.19	2.94	1.30	1.49	7.10	2.47	1.26	7.76	2.41	1.30	2.43	1.99
<b>Norton-Manipulation</b>	2.76	1.81	1.34	1.57	1.83	1.59	1.50	1.88	1.40	1.65	1.55	1.75
<b>Norton-LSE</b>	1.50	1.59	1.33	1.10	1.47	1.44	1.67	1.87	1.56	2.03	1.51	2.48
<b>Proposed</b>	0.72	0.87	0.68	0.81	0.75	0.74	0.81	0.79	0.81	0.85	0.92	0.73

**Table 7.** Comparisons between the proposed method and Norton-based methods w.r.t. MAE.

	3rd	5th	7th	9th	11th	13th	15th	17th	19th	21th	23th	25th
<b>Norton-Two points</b>	3.55	2.36	0.99	1.16	5.58	1.96	0.99	6.53	1.95	1.00	1.89	1.64
<b>Norton-Manipulation</b>	2.25	1.44	0.99	1.24	1.47	1.30	1.21	1.54	1.14	1.36	1.24	1.42
<b>Norton-LSE</b>	1.21	1.27	1.04	0.88	1.17	1.16	1.41	1.51	1.21	1.84	1.21	2.11
<b>Proposed</b>	0.58	0.68	0.52	0.66	0.60	0.59	0.63	0.61	0.64	0.69	0.75	0.59

**Table 8.** Comparisons between the proposed method and Norton-based methods w.r.t. Correlation Coefficient.

	3rd	5th	7th	9th	11th	13th	15th	17th	19th	21th	23th	25th
<b>Norton-Two Points</b>	−0.25	0.03	0.16	−0.11	−0.03	−0.01	0.07	0.19	−0.12	0.11	−0.08	−0.03
<b>Norton-Manipulation</b>	−0.25	−0.12	0.11	−0.10	0.01	0.04	−0.07	0.14	−0.04	0.14	0.01	0.07
<b>Norton-LSE</b>	0.35	0.18	0.16	−0.17	−0.03	0.02	0.00	0.10	0.03	−0.03	0.11	−0.08
<b>Proposed</b>	0.87	0.84	0.85	0.70	0.85	0.85	0.65	0.80	0.77	0.63	0.80	0.88

**Table 9.** Computation time consumed by the four methods.

	Norton-Two Points	Norton-Manipulation	Norton-LSE	Proposed
<b>Matlab/Simulink</b>	0.092	0.065	0.089	0.225
<b>Field Data</b>	0.017	0.039	0.021	0.070

#### 4. Discussion

Through the case studies for a single-phase rectifier simulation as well as for field measurements from a UHV-DC converter, the results evidenced that,

- (1) The proposed method presented better estimation accuracy than the three Norton-based methods;
- (2) Omitting of conjugate component in the coupled admittance model, that is,  $Y^- U^*$ , will decrease the accuracy of harmonic current estimation to a great extent;
- (3) The harmonic current in each order is impacted by harmonic voltage in different orders. Omitting the coupling relationships between harmonic voltage and current in different orders will decrease the estimation accuracy;
- (4) The computational complexity of the proposed method is higher than the three Norton-based methods.

#### 5. Conclusions

To identify the parameters in a coupled harmonic admittance model, this paper proposed a method based on Least Square Estimation using measurements of voltage and current. Through simulations for a single-phase bridge converter as well as field measurements from a converter station connected with a  $\pm 800$  kV 6400 MW UHVDC power transmission line, the accuracy of the proposed method was verified by comparing with three Norton-based identification methods.

In the future, aiming to estimate the impact of harmonics sources on the system voltage distortion, our research will focus on calculation of harmonic power flow based on the coupled harmonic admittance model.

**Author Contributions:** Methodology, Y.L., Z.D. and T.W.; Validation, Y.L., G.Z.; Formal Analysis, Y.L., T.W., S.Z.; Data Curation, S.Z.; Writing-Original Draft Preparation, Y.L.; Revision, Y.L., Z.D. and T.W.

**Funding:** This research was funded by State Grid Corporation of China (SGCC) Scientific and Technological Project Fund- Harmonic source analysis based on grid-wide harmonic monitoring data.

**Conflicts of Interest:** The authors declare no conflict of interest.

## References

1. Medina, A.; Segundo, J.; Ribeiro, P.F.; Xu, W.; Lian, K.L.; Chang, G.W.; Dinavahi, V.; Watson, N.R. Harmonic Analysis in Frequency and Time Domain. *IEEE Trans. Power Deliv.* **2013**, *28*, 1813–1821. [[CrossRef](#)]
2. Abdullah, A.R.; Peng, G.Z.; Ghani, S.A.; Jopri, M.H. A new vector draft method for harmonic source detection at point of common coupling. In Proceedings of the IEEE International Power Engineering and Optimization Conference, Langkawi, Malaysia, 24–25 March 2014; pp. 110–114. [[CrossRef](#)]
3. Dantona, G.; Muscas, C.; Sulis, S. Harmonic source estimation: A new approach for the localization of nonlinear loads. In Proceedings of the International Conference on Harmonics and Quality of Power, Wollongong, Australia, 28 September–1 October 2008; pp. 1–6. [[CrossRef](#)]
4. Wang, L.; Guo, S.F. Measurement Based on the “Group Linear Regression Method” of Harmonic Impedance. *Adv. Mat. Res.* **2011**, *354*, 1051–1057. [[CrossRef](#)]
5. Farhoodnea, M.; Mohamed, A.; Shareef, H. A single point measurement method for evaluating harmonic contributions of utility and customer in power distribution systems. *J. Appl. Sci.* **2011**, *11*, 257–265. [[CrossRef](#)]
6. Wang, X.; Blaabjerg, F.; Chen, Z.; Wu, W. Modeling and analysis of harmonic resonance in a power electronics based AC power system. In Proceedings of the 2013 IEEE Energy Conversion Congress and Exposition, Denver, CO, USA, 15–19 September 2013; pp. 5229–5236. [[CrossRef](#)]
7. Khazaei, J.; Beza, M.B.; Bongiorno, M. Impedance Analysis of Modular Multi-Level Converters Connected to Weak AC Grids. *IEEE Trans. Power Syst.* **2018**, *33*, 4015–4025. [[CrossRef](#)]
8. Unsar, O.; Salor, O.; Cadirci, I.; Ermis, M. Identification of harmonic current contributions of iron and steel plants based on time-synchronized field measurements—Part I: At PCC. In Proceedings of the 2013 IEEE Industry Applications Society Annual Meeting, Lake Buena Vista, FL, USA, 6–11 October 2013; pp. 4336–4347. [[CrossRef](#)]
9. Unsar, O.; Salor, O.; Cadirci, I.; Ermis, M. Identification of harmonic current contributions of iron and steel plants based on time-synchronized field measurements—Part II: Inside plants. In Proceedings of the 2013 IEEE Industry Applications Society Annual Meeting, Lake Buena Vista, FL, USA, 6–11 October 2013; pp. 1–7. [[CrossRef](#)]
10. Trejos, A.; Gonzalez, D.; Ramospaja, C.A. Modeling of Step-up Grid-Connected Photovoltaic Systems for Control Purposes. *Energies* **2012**, *5*, 1900–1926. [[CrossRef](#)]
11. Farhoodnea, M.; Mohamed, A.; Shareef, H.; Zayandehroodi, H. An enhanced method for contribution assessment of utility and customer harmonic distortions in radial and weakly meshed distribution systems. *Int. J. Electr. Power Energy Syst.* **2012**, *43*, 222–229. [[CrossRef](#)]
12. He, J.; Li, Y.W.; Bosnjak, D.; Harris, B. Investigation and Active Damping of Multiple Resonances in a Parallel-Inverter-Based Microgrid. *IEEE Trans. Power Electron.* **2013**, *28*, 234–246. [[CrossRef](#)]
13. Wen, B.; Boroyevich, D.; Burgos, R.; Mattavelli, P.; Shen, Z. Inverse Nyquist Stability Criterion for Grid-Tied Inverters. *IEEE Trans. Power Electron.* **2017**, *32*, 1548–1556. [[CrossRef](#)]
14. Pereira, H.A.; Freijedo, F.D.; Silva, M.M.; Mendes, V.F.; Teodorescu, R. Harmonic current prediction by impedance modeling of grid-tied inverters: A 1.4 MW PV plant case study. *Int. J. Electr. Power Energy Syst.* **2017**, *93*, 30–38. [[CrossRef](#)]
15. Agbemuko, A.; Domínguez-García, J.; Prieto-Araujo, E.; Gomis-Bellmunt, O. Impedance Modelling and Parametric Sensitivity of a VSC-HVDC System: New Insights on Resonances and Interactions. *Energies* **2018**, *11*, 845. [[CrossRef](#)]
16. Chakrasali, R.L.; Sheelavant, V.R.; Nagaraja, H.N. Network approach to modeling and simulation of solar photovoltaic cell. *Renew. Sustain. Energy Rev.* **2013**, *21*, 84–88. [[CrossRef](#)]
17. Fan, R.; Tan, T.; Chang, H.; Tong, X.; Gao, Y. A Method for Assessing Customer Harmonic Emission Level Based on the Iterative Algorithm for Least Square Estimation. *Engineering* **2013**, *5*, 6–13. [[CrossRef](#)]
18. Supriya, P.; Nambiar, T.N. Performance evaluation of harmonic current estimation using independent component analysis. *J. Electr. Eng.* **2013**, *13*, 14–21.

19. Jordan, M.; Grumm, F.; Langkowski, H.; Do Thanh, T.; Schulz, D. Online Network Impedance Identification with Wave-Package and Inter-Harmonic Signals. In Proceedings of the 2015 International School on Nonsinusoidal Currents and Compensation (ISNCC), Lagow, Poland, 15–18 June 2015. [[CrossRef](#)]
20. Karami, E.; Madrigal, M.; Gharehpetian, G.B.; Rouzbehi, K.; Rodriguez, P. Single-Phase Modeling Approach in Dynamic Harmonic Domain. *IEEE Trans. Power Syst.* **2018**, *33*, 257–267. [[CrossRef](#)]
21. Jordan, M.; Thanh, T.D.; Langkowski, H.; Schulz, D. Harmonic network impedance identification with pulse response analysis. In Proceedings of the International Conference on Electric Power and Energy Conversion Systems, Istanbul, Turkey, 2–4 October 2013; pp. 1–6. [[CrossRef](#)]
22. Kwon, J.B.; Wang, X.; Blaabjerg, F.; Bak, C.L.; Sularea, V.S.; Busca, C. Harmonic Interaction Analysis in a Grid-Connected Converter Using Harmonic State-Space (HSS) Modeling. *IEEE Trans. Power Electron.* **2017**, *32*, 6823–6835. [[CrossRef](#)]
23. Jing, L.; Xin, Z.; Xu, C.; Molinas, M. Harmonic State-Space Based Small-Signal Impedance Modeling of Modular Multilevel Converter with Consideration of Internal Harmonic Dynamics. *IEEE Trans. Power Electron.* **2018**. [[CrossRef](#)]
24. Wang, T.; Li, Y.; Deng, Z.; Liu, Y.; Li, Y.; Tan, M.; An, Z. Implementation of state-wide power quality monitoring system in China. In Proceedings of the 2018 IEEE PES General Meeting, Portland, OR, USA, 5–9 August 2018.
25. Borkowski, D.; Wetula, A.; Bien, A. New method for noninvasive measurement of utility harmonic impedance. In Proceedings of the Power and Energy Society General Meeting, San Diego, CA, USA, 22–26 July 2012; pp. 1–8. [[CrossRef](#)]
26. Nassif, A.B.; Yong, J.; Xu, W. Measurement-based approach for constructing harmonic models of electronic home appliances. *IET Gener. Transmiss. Distrib.* **2010**, *4*, 363–375. [[CrossRef](#)]
27. Braga, D.S.; Jota, P.R.S. Prediction of total harmonic distortion based on harmonic modeling of nonlinear loads using measured data for parameter estimation. In Proceedings of the 2016 17th International Conference on Harmonics and Quality of Power (ICHQP), Belo Horizonte, Brazil, 16–19 October 2016. [[CrossRef](#)]
28. Sun, Y.; Zhang, G.; Xu, W.; Mayordomo, J.G. A Harmonically Coupled Admittance Matrix Model for AC/DC Converters. *IEEE Trans. Power Syst.* **2007**, *22*, 1574–1582. [[CrossRef](#)]
29. Fauri, M. Harmonic modelling of non-linear load by means of crossed frequency admittance matrix. *IEEE Trans. Power Syst.* **1997**, *12*, 1632–1638. [[CrossRef](#)]
30. Sun, Y.; Dai, C.; Li, J.; Yong, J. Frequency-domain harmonic matrix model for three-phase diode-bridge rectifier. *IET Gener. Transmiss. Distrib.* **2016**, *10*, 1605–1614. [[CrossRef](#)]
31. Fang, J.; Wang, Y.; Luan, L.; Li, S. Frequency domain harmonic model of electric vehicle charger using three-phase uncontrolled rectifier. In Proceedings of the China International Conference on Electricity Distribution, Xi'an, China, 10–13 August 2016; pp. 1–5. [[CrossRef](#)]
32. Yong, J.; Chen, L.; Chen, S.Y. Modeling of home appliances for power distribution system harmonic analysis. *IEEE Trans. Power Deliv.* **2010**, *25*, 3147–3155. [[CrossRef](#)]
33. Yong, J.; Chen, L.; Nassif Alexandre, B.; Xu, W. A frequency-domain harmonic model for compact fluorescent lamps. *IEEE Trans. Power Deliv.* **2010**, *25*, 1182–1189. [[CrossRef](#)]
34. Thunberg, E.; Soder, L. A Norton approach to distribution network modeling for harmonic studies. *IEEE Trans. Power Deliv.* **1999**, *14*, 272–277. [[CrossRef](#)]
35. Sheng, B.; Danielsson, J.; Fu, Y.; Liu, Z. Converter valve design and valve testing for Xiangjiaba–Shanghai  $\pm 800$  kV 6400 MW UHVDC power transmission project. In Proceedings of the IEEE International Conference on Power System Technology, Hangzhou, China, 24–28 October 2010; pp. 1–5. [[CrossRef](#)]
36. *National standard of China “Power Quality-Terms”*; GB/T 32507; China National Standards: Beijing, China, 2016.

